15ICGE - CONFERENCE PROCEEDINGS
15th International Conference on Geotechnical Engineering
December 5-7, 2019, Lahore, Pakistan
*Invited Keynote Lecture*

# USE OF RUBBER TYRE ELEMENTS IN TRACK STABILIZATION

**Buddhima Indraratna [1], Yujie Qi [2], Chamindi Jayasuriya [3], Ana Ribeiro Heitor [4], and Sinniah K. Navaratnarajah [5]**

*1) Distinguished Professor of Civil Engineering; Research Director, Centre for Geomechanics and Railway Engineering, and ARC Training Centre for Advanced Technologies in Rail Track Infrastructure, University of Wollongong, Australia*
*2) Research Associate, Centre for Geomechanics and Railway Engineering, and ARC Training Centre for Advanced Technologies in Rail Track Infrastructure, University of Wollongong, Australia*
*3) Research Associate, Centre for Geomechanics and Railway Engineering, and ARC Training Centre for Advanced Technologies in Rail Track Infrastructure, University of Wollongong, Australia*
*4) Senior Lecturer, Centre for Geomechanics and Railway Engineering, and ARC Training Centre for Advanced Technologies in Rail Track Infrastructure, University of Wollongong, Australia*
*5) Senior Lecturer, Department of Civil Engineering, University of Peradeniya, Sri Lanka*
*indra@uow.edu.au, qyujie@uow.edu.au, chamindi@uow.edu.au, aheitor@uow.edu.au, navask@eng.pdn.ac.lk*

**Abstract:** Ballasted rail tracks are common in many countries because of their excellent load-bearing capacity, good drainage and economic benefits. To meet the increasing demand for passenger and freight transportation via rail, operations of high-speed heavy haul trains have become a necessity. However, the increase in dynamic stresses of rail traffic progressively degrades the primary load-bearing ballast layer, which inevitably leads to excessive settlement and instability, damage to track elements, and more frequent and costly maintenance. In recent years, the use of energy absorbing inclusions in rail track foundations has become increasingly popular because their high damping properties help to reduce track degradation and vibrations caused by moving trains. This keynote paper showcases several recent research studies carried out at the University of Wollongong to evaluate the role of recycled rubber tyre products (e.g. tyre cells, under sleeper pats, under ballast mats, and rubber crumbs) in improving rail track performance. In view of this, large scale laboratory tests have been conducted using state-of-the-art facilities designed and built at the University of Wollongong. Based on these tests, the load-deformation behaviour of ballast and subballast enhanced by the energy absorbing inclusions have been analysed. In addition, test data from the capping layer confined with a tyre cell and the inclusion of rubber mats in the track substructure has also been validated by Finite Element Modelling (FEM). The results from these large-scale laboratory tests and numerical modelling indicate that the use of resilient rubber inclusions substantially improve track behaviour.

## 1. INTRODUCTION

Ballasted rail tracks play an important role in transporting freight and passengers worldwide. In recent years railway industries have placed a greater emphasis on construction of high-speed train corridors and implement heavier freight operations to achieve more efficient and cost-effective services, particularly in the mining and agricultural sectors (Indraratna et al. 2018, Indraratna et al. 2019). However, higher speeds and heavier loads accelerate track degradation, especially in the ballast layer, which inevitably results in frequent and costly track maintenance. The ballast layer usually consists of crushed, angular and uniformed hard rockfill or stone; it is the layer placed underneath the sleeper and on top of the subballast layer to provide structural support against the loads imposed by moving train wheels (Suiker et al. 2005, Indraratna et al. 2012, Sun et al. 2015). During the service life of rail tracks, ballast will progressively deteriorate due to the loss of angular corners and sharp edges, the intrusion of fines, and mud-pumping from the underlying layers of subgrade.

To improve track stability and reduce ballast degradation due to increased vibration and cyclic loads, the inclusion of energy absorbing materials such as rubber mats, tyre cells, and rubber crumbs becomes increasingly popular high damping property of rubber materials. These properties help to attenuate the dynamic loads and vibrations that are generated under operating conditions and subsequently mitigate ballast deformation and degradation, with obvious implications for improved track stability and longevity (Schneider et al. 2011, Costa et al. 2012, Nimbalkar et al. 2012, Sol-Sánchez et al. 2015, Indraratna et al. 2017a, Indraratna et al. 2017b, Navaratnarajah and Indraratna 2017, Qi et al. 2017, Qi et al. 2018, Indraratna et al. 2019). Furthermore, since these energy absorbing rubber products can be obtained from end-of-life tyres, it is environmentally friendly and economically attractive to reuse them in geotechnical projects. Despite these obvious advantages,

current literature on the application of energy absorbing rubber materials to improve track performance is still very limited.

Several types of waste tyre products can be used in rail foundations: (i) rail pads installed at the interface of sleeper and the rail; (ii) under sleeper pats (USP) placed underneath the sleeper (Navaratnarajah et al. 2018, Jayasuriya et al. 2019); (iii) under ballast mats (UBM) installed between the ballast and subballast (Navaratnarajah and Indraratna 2017); (iv) tyre cells to reinforce the subballast layer (Indraratna et al. 2017b, Indraratna et al. 2017c); and (v) mixing rubber crumbs with ballast for the ballast layer or blending them with other waste materials for the subballast layer (Sol-Sánchez et al. 2015, Indraratna et al. 2017a, Qi et al. 2017).

This paper reviews the current state-of-the-art studies on the applications of energy absorbing rubber products in rail foundations undertaken at the University of Wollongong (Australia); they include, (i) developing a synthetic energy absorbing layer for subballst using waste mixtures (SFS+CW+RC matrix); (ii) improving track degradation by using USP and UBM; and (iii) reinforcing the subballast layer with waste tyre cells. A schematic optimization system is proposed to help select the optimal waste matrix for the subballast layer. Large scale cubical triaxial tests have been carried out to investigate the performance of USP, UBM and tyre cells in rail tracks, and analysis via finite element modelling (FEM) is used to examine the behaviour of USP and tyre cell-reinforced subballast. These research outcomes are expected to contribute to better design solutions by considering the role of how energy absorbing materials will enhance track stability and longevity and also reduce the maintenance costs.

## 2. A SYNTHETIC ENERGY ABSORBING LAYER USING WASTE MATRIX FOR RAILWAY SUBBALLAST

### 2.1 Materials and Test Program

The source materials for SFS and CW are from ASMS (Australia Steel Milling Services) and Illawarra Coal Mining, respectively. The RC shredded from waste tyres from Tyre Crumbs Australia come in three different sizes (0-2.3mm, 0.3-3mm, and 1-7 mm). According to the unified soil classification system, SFS and CW are classified as well-graded gravel with silty-sand (GW-GM), and well-graded sand with gravel (SW), respectively, whereas RC is referred to as granulated rubber (ASTM-D6270 2008). The particle size distribution (PSD) curves of SFS, CW, and RC are shown in Figure 1. The SFS and RC materials are sieved by the dry method, whereas the CW is sieved by the wet method to prevent fine particles from adhering to the larger particles.

To optimise the SFS+CW+RC matrix as suitable railway subballast, eight parameters are considered based on the existing evaluation criteria for traditional subballast materials and the adverse geotechnical properties of these three waste materials. These eight parameters are then divided into three categories: (i) the gradation, shear strength, and hydraulic conductivity which guarantee the three main functions of the subballast layer (i.e. filtration, stress distribution and drainage); (ii) the swell pressure, breakage index (BI), axial strain under cyclic loading, and resilient modulus, all of which aim at controlling the adverse geotechnical properties of these three waste materials, i.e., the volumetric expansion of SFS, the particle breakage of CW, and the high deformation of rubber crumbs; (iii) the strain energy density (E) to evaluate the energy absorbing properties of the waste matrix. The comprehensive laboratory tests undertaken to examine these parameters include permeability tests, swell tests, and consolidated triaxial tests under static and cyclic loading conditions.

To prevent the influence of gradation, all the waste mixtures were mixed with the same PSD (the target PSD, Figure 1) chosen by Indraratna et al. (2017a) on the basis of traditional subballast gradation in Australia. All the waste mixtures were blended by weight because the by-weight percentage is more accurate during sample preparation (Edil and Bosscher 1994, Feng and Sutter 2000). The RC content ($R_b$,%) in the matrix was not more than 40% to prevent the sample skeleton from being totally controlled by RC (Kim and Santamarina 2008, Senetakis et al. 2012). The blending ratio of SFS:CW was set to 5:5, 7:3, and 9:1. All the test specimens were blended to their optimum moisture content and then compacted to 95% of their maximum dry unit weight; the effective confining pressure $\sigma'_3$ for these triaxial tests were 10, 40, and 70 kPa to simulate the field conditions of railway subballast. The test procedures have been described in detail by Indraratna et al. (2017a).

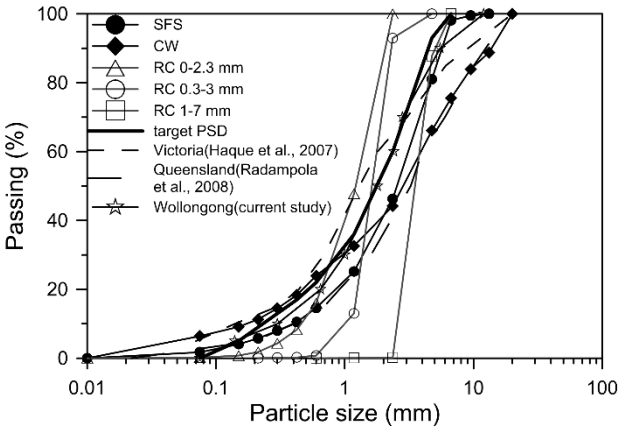


Figure 1 Particle size distribution (PSD) curves of the waste materials and selected PSD for the waste matrix (modified after Indraratna et al. 2017a).

### 2.2 Optimization of the Waste Matrix

The optimum waste matrix for subballast is chosen by obtaining the optimal SFS:CW firstly and then determining the optimal amount of RC. It is reported that the hydraulic conductivity, energy-absorbing properties and particle breakage of all the blended mixtures with $R_b \geq 10$ % and SFS:CW≥5:5 are superior to traditional subballast materials (Indraratna et al. 2017a). However, a higher content of SFS increases the volumetric expansion, and a higher proportion of CW reduces the shear strength, i.e. the blending ratio of

SFS:CW is the main factor controlling the strength and the volume expansion of the matrix. Therefore, the optimal SFS:CW is determined by the test results of the swell pressure ($P_{swell}$) and peak friction angle ($\emptyset'_{peak}$ ) of the waste matrix having 10% RC (Figure 2). To guarantee that the optimum mixture has sufficient shear strength and less swell pressure than the minimum vertical loads applied to the capping layer, the waste mixtures should satisfy $\emptyset'_{peak} \geq 49°$ (Indraratna et al. 2017a) and $P_{swell} < 30kPa$ (Ferreira et al. 2010), therefore an SFS:CW = 7:3 is chosen as the optimal mixing ratio for SFS and CW.

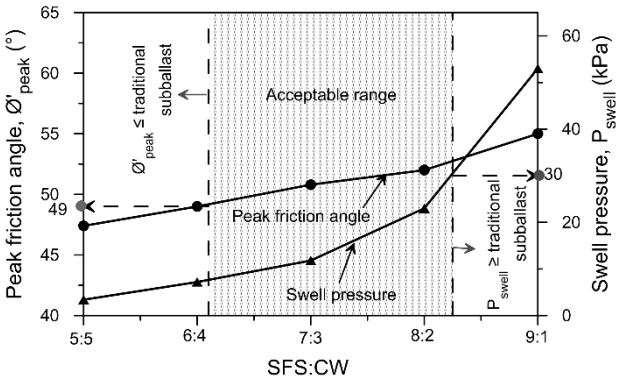


Figure 2 Optimising the blending ratio of SFS:CW (modified after Indraratna et al. 2017a)

The optimal $R_b$ is evaluated in accordance with the test results of breakage index, peak friction angle, resilient modulus, strain energy density, swell pressure, and axial strain obtained under cyclic loading of the waste matrix with SFS:CW=7:3 (Figure 3). Figure 3a shows that only mixtures with $R_b$ from 8~18.5% satisfy the required range based on particle breakage (BI≤2%, Indraratna et al. 2017a) and shear strength ($\emptyset_{peak} \geq 49°$). Figure 3b shows that only the waste matrix with $R_b$ falling between 2~18% will satisfy the requirements of an axial strain under cyclic loading (≤ 2%) and swell pressure ($P_{swell} < 30kPa$). The test results from the strain energy density and resilient modulus indicate that the optimal amount of RC should be less than 15% (Figure 3c) and therefore the combined and acceptable amount of RC in the waste mixtures when all the above-mentioned parameters are considered should be between 8~15%. It is noteworthy that 10% of RC is enough to improve the energy-absorbing capacity of the waste matrix without influencing significantly the axial displacement and associated shear strength under static and cyclic loading conditions (Indraratna et al. 2017a, Qi et al. 2017). In this context, 10% of RC is the optimal amount of RC, and thus the optimum mixture would be SFS63+CW27+RC10 (SFS:CW=7:3, and 10% RC).

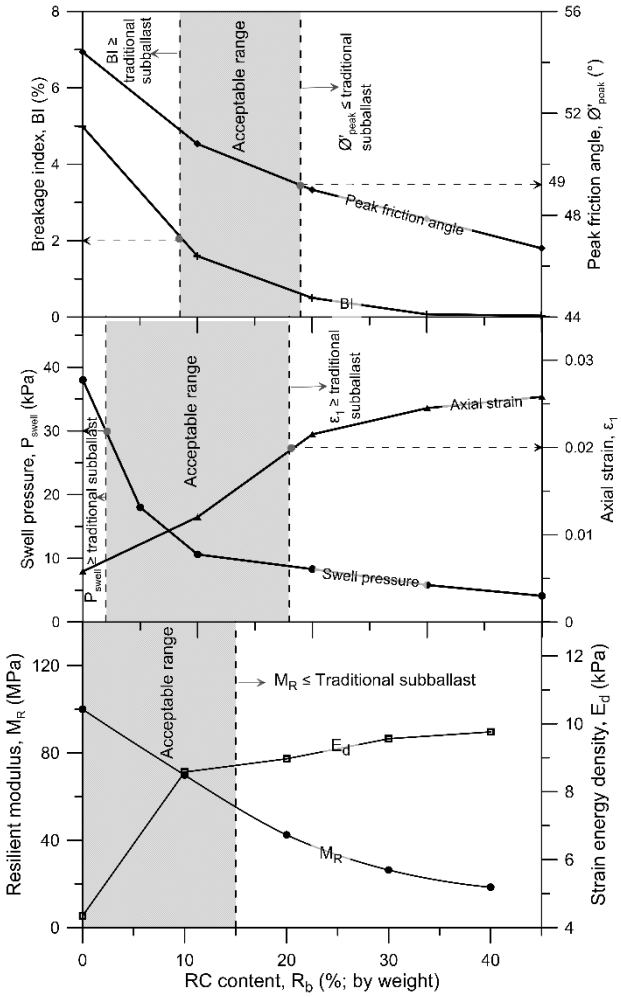


Figure 3 Optimising the RC content (modified from Indraratna et al. 2017a)

## 2.3 Energy-absorbing Analysis

If the total energy input by a given track load is assumed to be a certain amount, the energy applied to the ballast and the subgrade will decrease by increasing the energy absorbing capacity of the subballast layer, and thus reducing the particle breakage of ballast.

As shown in Figure 4, an energy consumption flowchart is established based on the comprehensive test results of the waste matrix. Here, the energy absorbed by the synthetic energy absorbing layer (SEAL) from the dynamic loading generally results in permanent deformation or is dissipated by heat and particle breakage. It is noted that as RC contents increase, the energy absorbed by the SEAL increases as the area of the shear stress-shear strain triangle increases (Figure 4a). This indicates that less energy will be transmitted to subgrade or the ballast layer, but accordingly, this energy results in permanent strains (Figure 4b) and the dissipated energy increases (Figure 4c). The dissipated energy represented by the area of the hysteresis loop obtained from cyclic loading tests is due to: (i) the recoverable deformation of the waste matrix, (ii) particle friction, and (iii) particle breakage (Feng and Sutter 2000, Li et al. 2016). Recoverable deformation is reflected by the resilient modulus $M_R$. Noted that the increase in dissipated energy is mainly due to the rise in the recoverable deformation ($M_R$ decreases, Figure 4d) as the shear strength (Figure 4e) and particle breakage (Figure

4f) decrease when the amount of RC increases.

This analysis reveals that using more rubber ensures the SEAL (SFS+CW+RC mixtures) has a higher energy absorbing capacity and less particle breakage, but higher deformation, lower resilient modulus, and less shear strength. Note that 10% of RC already has a promising energy absorbing capacity and therefore 10% RC is now proven to be the optimal amount of RC needed for the optimum waste matrix of subballast.

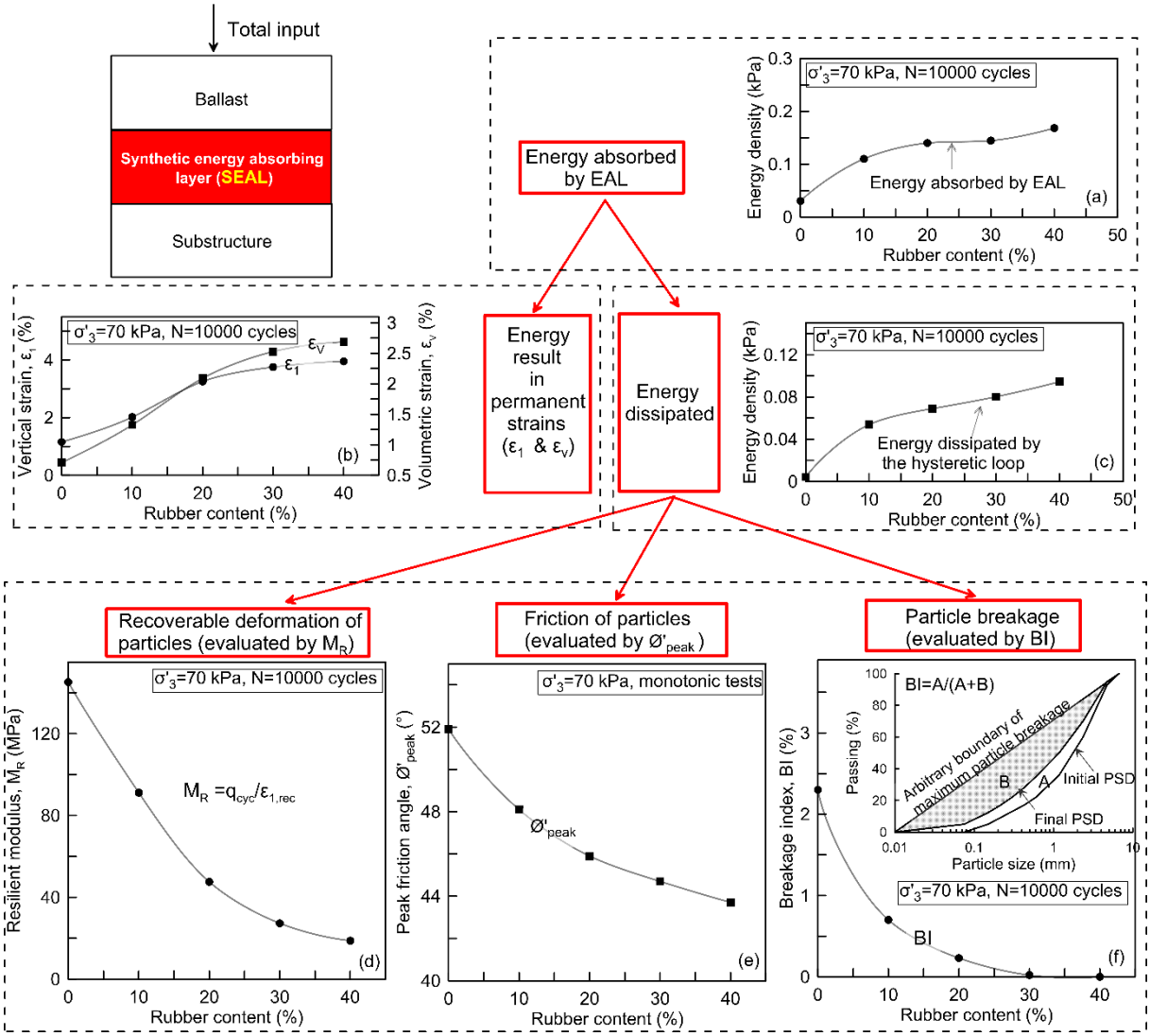


Figure 4 Energy-consumption flowchart and comprehensive properties of SFS+CW+RC mixtures (SFS:CW=7:3) having different amounts of RC s at effective confining pressure $\sigma'_3 = 70\ kPa$ and at loading cycles N=10,000 (modified after Qi et al. 2017)

## 3. LABORATORY INVESTIGATION BASED ON LARGE-SCALE TRIAXIAL TESTS

### 3.1 Under Sleeper Pats (USP) and Under Ballast Mats (UBM)

#### 3.1.1 Instrumentation for Specimen Preparation and Data Acquisition

A series of tests to investigate the effect and influence of rubber mats, have been carried out in the large-scale process simulation primoidal testing apparatus (PSPTA) designed and built at the University of Wollongong. Fresh ballast consists of aggregates crushed from latite (volcanic) basalt; the ordinary igneous rock used for experiments are from Bombo Quarry, NSW. The properties of ballast such as its strength, mineralogy, and flakiness, etc., are analysed in our laboratory, and the particle size distribution is according to the Australian Standard (AS-2758.7 2015). These fresh ballast aggregates have been cleaned with water; air dried, screened through selected sieve sizes, and then mixed in the desired proportion to obtain the test specimens. The integrated layers of substructure built inside the cubicle chamber that are shown in Figure 5 (a-b) of the PSPTA consist of rails, a concrete sleeper, ballast, and base (subballast or concrete slab). Three types of substructure are simulated in the laboratory test: (i) a regular open track where subballast is the base layer that is tested with and without USP under the concrete sleepers, (ii) a track on a bridge deck by placing a concrete slab as the base layer and tested with and without USP, and

(iii) track on a bridge deck by placing a concrete slab as the base layer and tested with and without UBM.

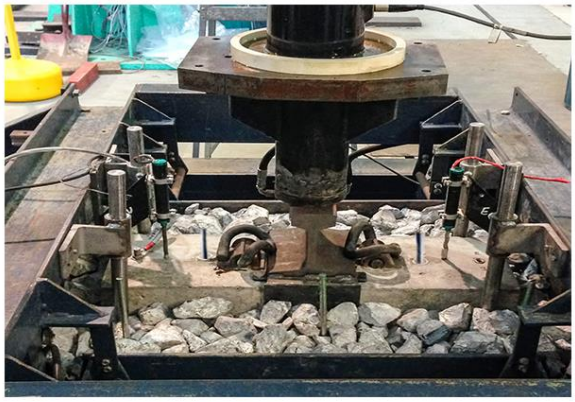

(a)

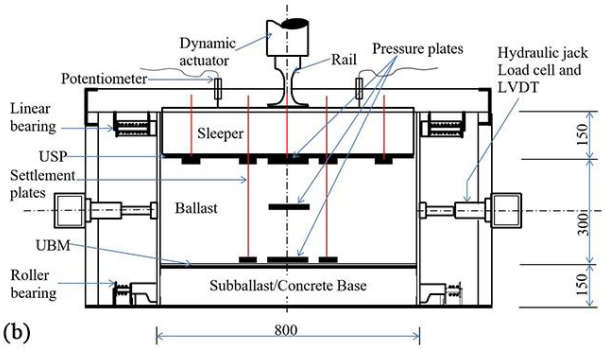


(b)

Figure 5 (a) Test sample prepared inside the testing chamber; and (b) Cross section of the testing chamber

Laboratory tests carried out with and without rubber mats where two different bases are placed under the ballast layer is shown in Figure 5(b). With an open track, the bottom layer of the test specimen consists of 150 mm thick subballast (compacted to around 95% of its maximum dry density with a rubber padded vibratory hammer) overlain by a 300 mm thick layer of ballast. When track on a stiff subgrade is considered, the subballast is replaced with a 150 mm thick concrete base to simulate a hard subgrade. Initially, the 150 mm thick subballast or concrete base is placed inside the test chamber and then fresh ballast is placed on top of the subballast or the concrete base, but when testing with UBM, a rubber mat is placed on top of the concrete base. Fresh ballast is placed as three 100 mm thick, compacted layers. The representative ballast aggregates directly under the sleeper in each 100 mm thick layer (bottom, middle and top) are colour coded as red, green, and blue, while the other aggregates below the sleeper are painted yellow and ballast above the sleeper (crib ballast) are painted white. Each layer of ballast is compacted to a typical field density of 1560 kg/m3 (this corresponds to the approximate initial void ratio, $e_0 = 0.73$ and specific gravity $G_s = 2.7$ for ballast) with a rubber padded vibratory compactor.

The rail-sleeper assembly is then placed at the top and in the centre of the compacted 300 mm load bearing ballast layer, and the space around the sleeper is filled and compacted with 150 mm thick crib ballast. When testing with USP, the pad is tightly glued to the bottom face of the concrete sleeper. A total of 500,000 load cycles (N) is applied for each test. The performance of this integrated layered track simulated in the laboratory is monitored in real time with robust and high-precision instruments such as load cells, Linear Variable Differential Transformers (LVDTs), potentiometers, pressure cells, and settlement plates; their initial readings are taken before starting the cyclic loading phase, and then continuous, high-frequency data and data at selected cycles (N=100, 500, 1000, 5,000, 10,000, 50,000, 100,000, 200,000, 300,000, 400,000 and 500,000) is collected from all the instruments via data loggers and host computers. Manual data is also collected at the aforementioned selected cycles. The final weight of each layer of ballast (after screening through selected sieves as per the PSD) is then measured and recorded for ballast breakage calculations.

The typical cyclic loading experienced by rail track foundations is simulated in the PSPTA. The cyclic load applied by the servo-hydraulic actuator through a 100 mm diameter cylindrical steel ram is transmitted to the ballast layer by the rail-sleeper assembly. The harmonic sinusoidal loading (cyclic major principal stress, $\sigma_{1,cyc}$) applied is shown in Figure 6.

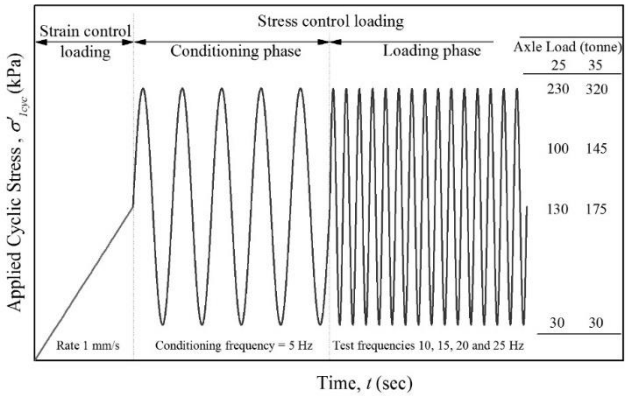


Figure 6 Cyclic loading conditions

As shown in Figure 7, 26 large-scale cyclic load tests have been carried out using PSPTA, of which eight were to analyse the performance of ballast with and without USP by simulating an open track where the subballast is under the ballast layer. The two simulated axle loads are 25 and 35t at loading frequencies of 15 and 20 Hz. Six tests were carried out to analyse the performance of ballast with and without USP on track with stiff subgrade and a 25t axle load with loading frequencies of 15, 20 and 25 Hz. The performance of UBM is analysed by simulating a hard base condition such as rail track running on a concrete bridge deck. There are twelve tests, with and without UBM on top of the concrete base and under the ballast layer. The simulated axle loads are 25t, with loading frequencies of 15, 20 and 25 Hz, and 35t with loading frequencies of 10, 15 and 20 Hz.

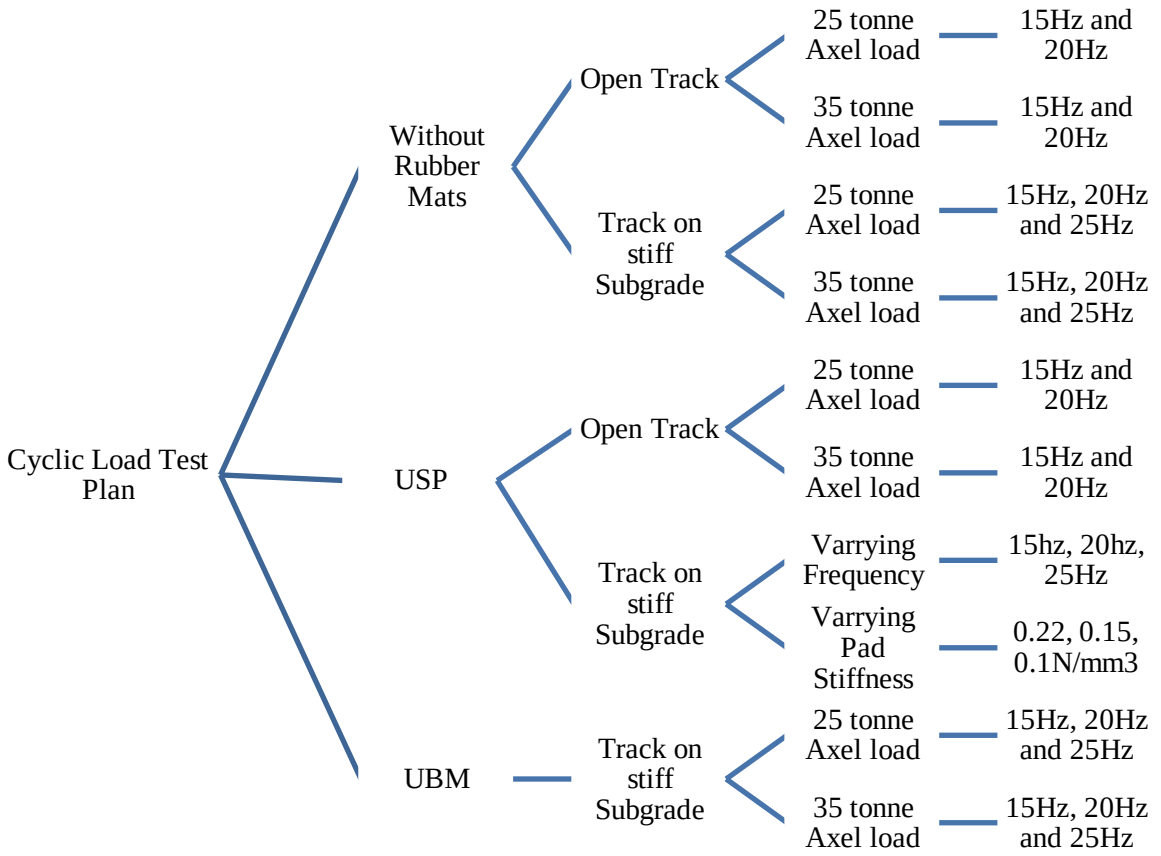


Figure 7 Experimental plan

**3.1.2 Performance of Ballast Stabilized with USP**

The vertical and lateral plastic deformation of ballast in an open track (and strain) with and without USP, and with 25t and 35t axle loads, is shown in Figures 8-9, respectively. Figure 10 shows the variations in the plastic deformation of ballast (on stiff subgrade) with and without USP and at varying frequencies, for a 25t axle load. The results indicate that ballast deforms rapidly up to around 10,000 cycles due to its initial densification and further packing after the corners of the sharp angular aggregates begin to break, but once the ballast begins to stabilise, the rate of deformation gradually decreases and then remains relatively constant after 100,000 cycles. This shows that ballast aggregates undergo considerable particle rearrangement and densification during the initial cycles, but after reaching a threshold compression, any subsequent load cycles will resist further deformation.

It is evident that the vertical and lateral ballast deformation decreases significantly by using USP in open tracks. This is because the increased contact area at the sleeper/ballast interface due to the USP at the sleeper-ballast interface reduces the induced stresses at the interface and at the particle-particle contact, and allow for a more uniform distribution of stress which in turn decreases the overall deformation. For the open track case, with limited loading frequencies of 15 and 20 Hz tested in this study, the vertical strain decreases in the range of 19-29% for a 25t axle load, and about 21% for a 35t axle load when USP is used with the concrete sleeper. The lateral strain decreases in the range of 9-14% for a 25t axle load and 9-11% for a 35t axle load.

As shown in Figure 10, any increase in train speed (increased frequency) increases the vertical and lateral displacement of the ballast layer (i.e. increasing the corresponding strains $\varepsilon_1$ and $\varepsilon_3$). As train speed increases, more kinetic energy is transmitted to the track foundation, so the subsequent ballast breakage, particle rearrangement, and densification leads to a significant increase of irrecoverable (plastic) deformation, but when USP is used there is a huge reduction in the permanent deformation of ballast on stiff subgrade. Figure 10 shows that USP can reduce the permanent vertical displacement $S_v$ from 16-47 % and decrease the lateral plastic displacement $S_L$ from 21-55%.

Progressive particle degradation occurs when a repetitive cyclic load is applied to the ballast mass. Initially, grinding and corner breakage of angular ballast at the sleeper-ballast interface and inter-particle contacts takes place, followed by complete fracture across the body of the particles, depending on the strength of the parent rock and the level of stress increment (Indraratna et al. 2005, Lackenby et al. 2007). This breakage of ballast particles contributes to increased axial and lateral strains and also causes differential track settlement. The BBI for each top, middle and bottom layers is shown in Figure 11 for ballast tested with and without USP, and for 25 and 35t axle loads, respectively. As expected, ballast breakage is greater at the top layer due to the higher interface and inter-particle contact stress at the top; this is

followed by the middle and then the bottom layers. This current study indicates there is less ballast degradation is when USP is used under concrete sleepers, in fact when all three layers are considered, USP reduces degradation by more than 50%. When each layer of ballast is considered separately, when 25t and 35t axle loads are tested at 15 and 20 Hz, the reduction of ballast degradation is between 53-63% for the top layer, between 51-59% for the middle layer, and between 48-62% for the bottom layer. The increased contact area due to USP and the subsequent reduction in the interface and inter-particle ballast stress is probably the main reason for this substantial reduction in ballast breakage.

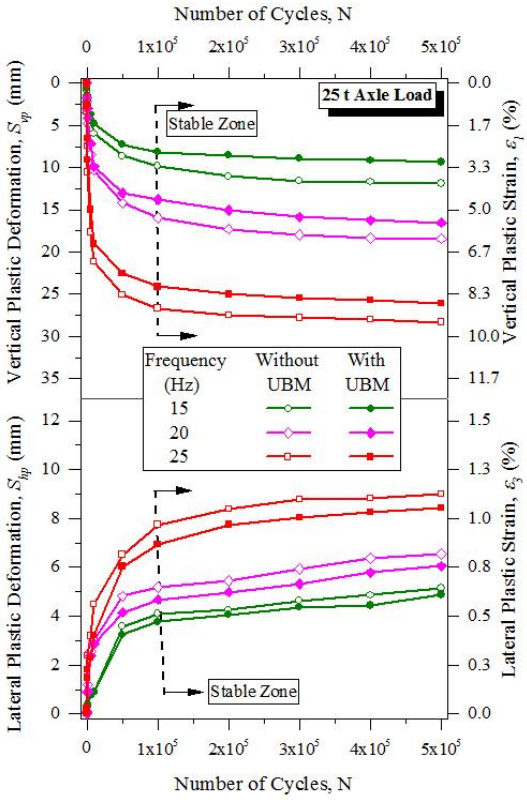


Figure 8 Test results of vertical and lateral plastic deformation of ballast with and without USP for 25t Axle Load (modified after Navaratnarajah et al. 2018)

Figure 12 shows the variations of BBI with loading frequency in the track with a stiff subgrade. Our experiments indicate that USPs reduce ballast particle degradation quite significantly, although an increase in train speed led to a gradual increase in the BBI and the loading frequency, whether or not USP is used. The level of energy transmitted to the ballast increases with the train speed and therefore there is more degradation under a higher loading frequency. There is a substantial reduction in particle breakage when USPs are present (the BBI decreases by 50-60%) because they absorb part of the energy transmitted to the ballast, and therefore the stress imparted onto the aggregated particles decreases, as does the subsequent abrasion, attrition, and breakage. Moreover, the contact area between sleeper and ballast helps to reduce the pressure that develops on the ballast, and therefore there is a reduction in ballast degradation.

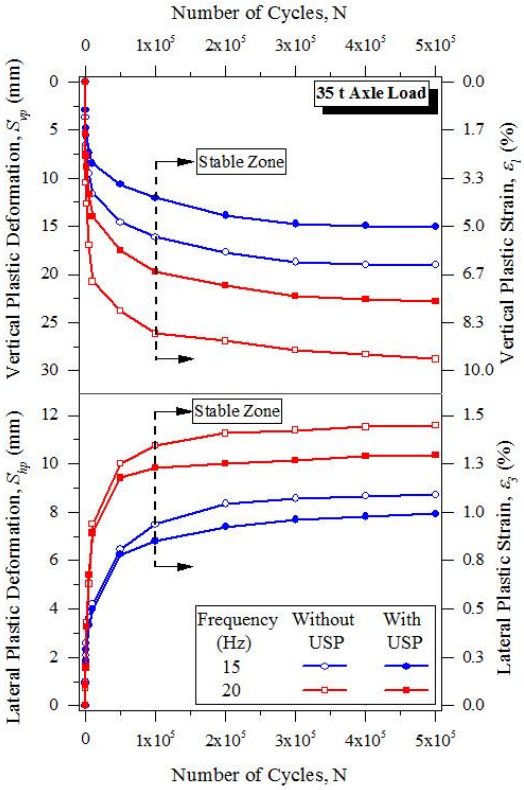


Figure 9 Test results of vertical and lateral plastic deformation of ballast layer with and without USP for 35t Axle Load (modified after Navaratnarajah et al. 2018)

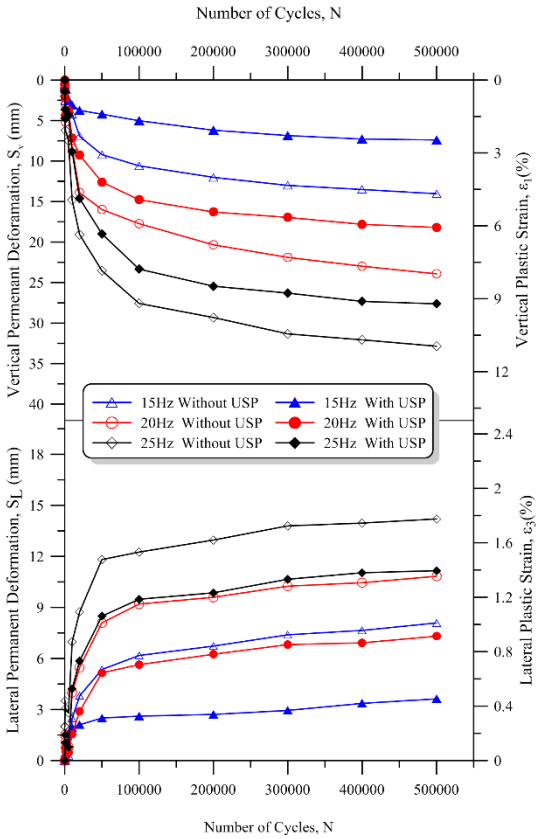


Figure 10 Test results of vertical and lateral plastic deformation of ballast layer with and without USP with varying frequencies (modified after Jayasuriya et al. 2019)

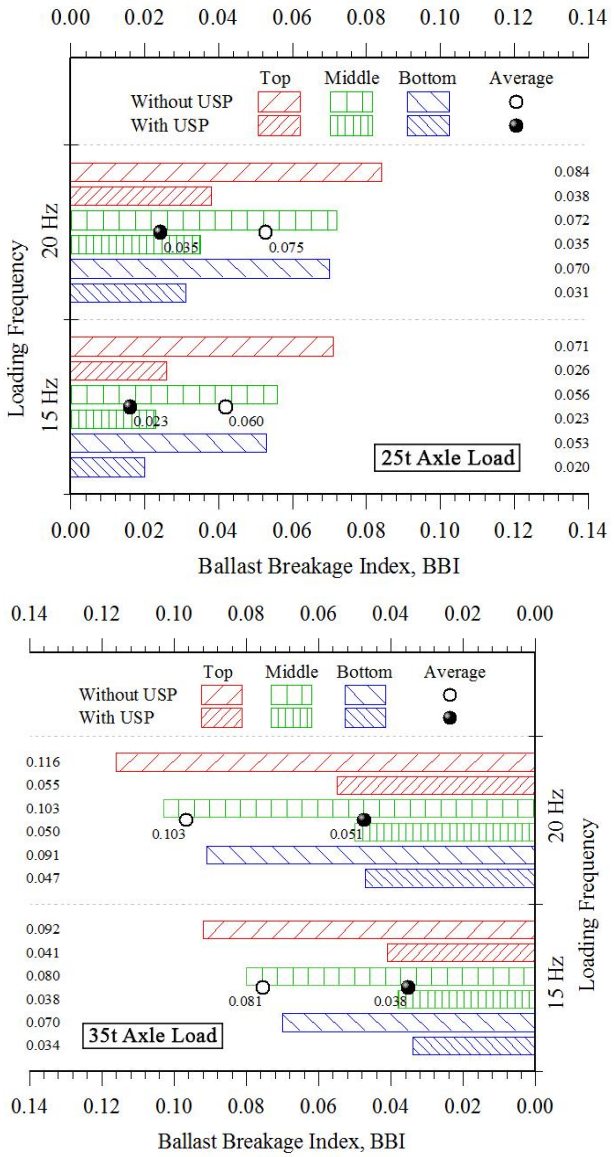


Figure 11 Variation of BBI of ballast layer in open track with and without USP (modified after Navaratnarajah et al. 2018)

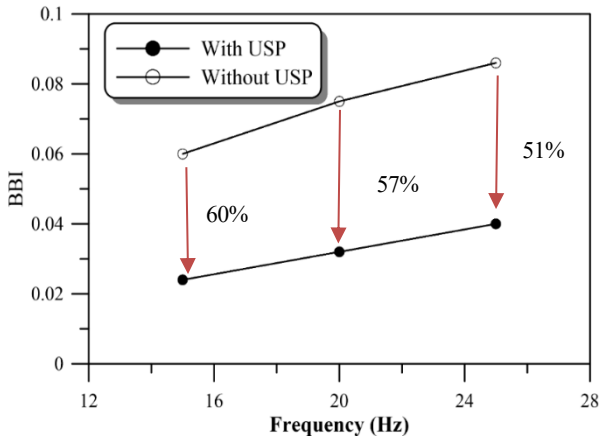


Figure 12 Variation of BBI with loading frequency and Reduction of BBI with the introduction of USP in ballasted track on stiff subgrade (modified after Jayasuriya et al. 2019)

### 3.1.3 Performance of Ballast Stabilised with UBM

The accumulated vertical and lateral plastic deformation (and strain) with and without UBM for 25t and 35t axle loads are shown in Figures 13-14, respectively. Like the test with USP, under every load, frequency, and UBM condition, the ensuing plastic deformation of ballast is rapid up to about 10,000 loading cycles, after which the rate of settlement gradually decreases until loading reaches about 100,000 cycles, after which it remains stable with almost constant settlement.

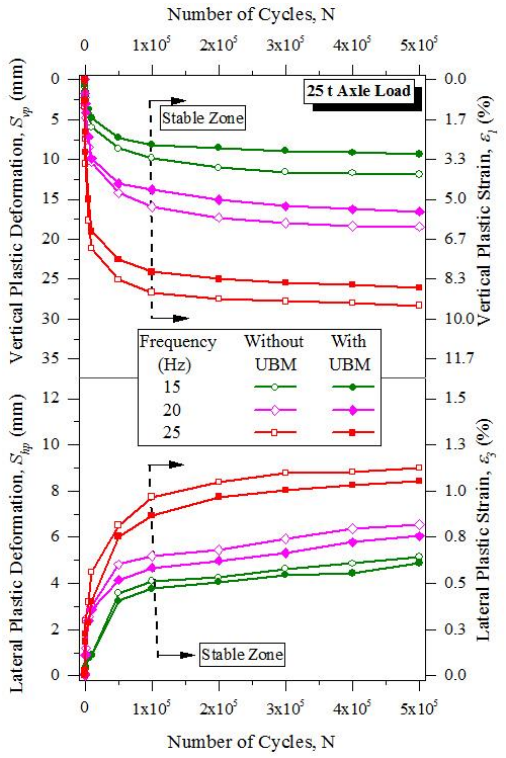


Figure 13 Variation of vertical and lateral plastic deformation with the number of cycles (N), and with and without UBM for 25t Axle Load (modified after Navaratnarajah and Indraratna 2017)

The results shown in Figures 13-14 indicate that UBM can reduce the overall plastic deformation of ballast when placed on top of a stiff base. This study also indicates that 10-20% reduction in vertical plastic deformation and a 5-10% reduction in lateral plastic deformation can be attained. However, these reductions in plastic deformation are highly dependent on the thickness, stiffness, and density of the rubber mat, and the stiffness of the formation, e.g. soft subgrade versus stiff formation. In this study, relatively dense 10 mm thick (static stiffness 0.2 N/mm$^3$) rubber mats were used on top of the concrete base. In actual practice, UBMs are more effective when the support is stiffer, such as in tunnels and on concrete bridges. Increasing the thickness of the elastic layer or using an elastic element to reduce the stiffness beyond an optimum value can lead to excessive plastic deformation of ballast, as well as fatigue damage to other track components (Hunt and Wood 2005). Therefore, the thickness, stiffness, and density of a UBM with respect to the stiffness of the formation are crucial in reducing the vibration and

plastic deformation of ballast.

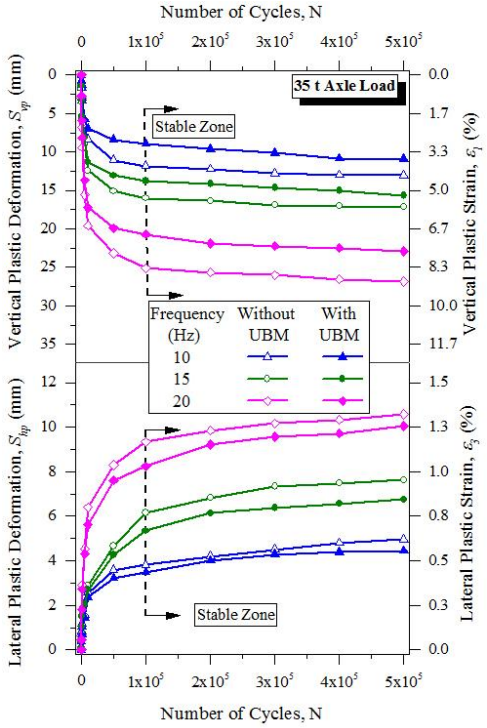


Figure 14 Test results of vertical and lateral plastic deformation of ballast layer with and without UBM for 35t Axle Load (modified after Navaratnarajah and Indraratna 2017)

The quantified values of ballast degradation (BBI) are presented in Figures 15-16 for 25t and 35t axle loads, respectively, with varying loading frequencies (10 to 25 Hz) for ballast with and without UBM placed on top of a hard concrete base. As expected, ballast degradation is higher in the top layer; there is less degradation in the middle layer and even less at the bottom as the induced cyclic stress decreases with depth. Figures 15-16 also show that ballast degradation decreases significantly when there is a UBM on top of a hard concrete base; when all three layers are considered, this study shows an average 35-45% reduction of breakage. When individual layers are considered, there is about 50-60% reduction of BBI at the bottom layer compared to 20-25% and 30-50% at the top and the middle layers, respectively. This clearly demonstrates how UBMs on a concrete base (or stiff subgrade such as bedrock) help to reduce ballast breakage.

### 3.2 Tyre Cell-reinforced Capping Layer

#### 3.2.1 Materials and Test Loading Conditions

An innovative method of confining the capping layer (subballast) using recycled tyre cells has been proposed by (Indraratna et al. 2017c), with the aim of reducing particle movement and ballast degradation and increasing the stability and resiliency of track infrastructure. Large-scale cyclic loading triaxial tests to evaluate the tyre cell-confined capping layer using PSPTA have been carried out. To simulate the a track foundation under field conditions, a simplified 600×800 mm and 600 mm high unit cell is installed in the PSPTA. This large-scale triaxial sample consists of 3 layers, i.e. ballast layer, a capping layer, and a subgrade layer (Figure 17). The ballast and capping layers are crushed basalt (latite) with the particle size ranging from 2.36-53 mm and 0.075-19 mm, respectively. The capping layer is confined with or without rubber tyres (one side wall removed). The bottom layer is a 50-mm thick compacted rockfill base that can simulate a typical structural fill.

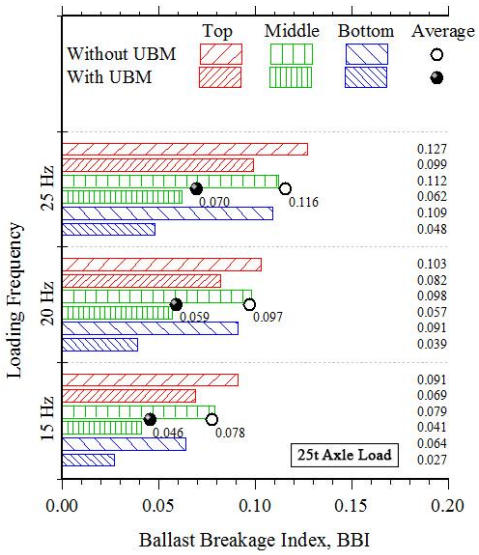


Figure 15 Variation of BBI for 25t Axle Load with and without UBM (modified after Navaratnarajah and Indraratna 2017)

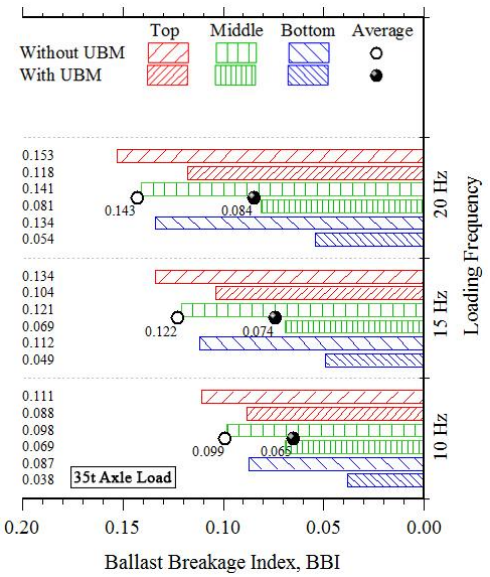


Figure 16 Variation of BBI for 35t Axle Load with and without UBM (modified after Navaratnarajah and Indraratna 2017)

The cyclic loading tests are carried out under a frequency of 15 Hz to simulate a train travelling at approximately 110 km/h (Indraratna et al. 2014). A maximum axial stress $\sigma'_{1cyc,max} = 385\ kPa$ and a minimum axial stress $\sigma'_{1cyc,min} = 15\ kPa$ are applied to simulate an axle load of 40 tonnes (Jeffs and Tew 1991). Each cyclic loading test

consists of 500,000 cycles, after which the ballast is sieved to determine the extent of degradation.

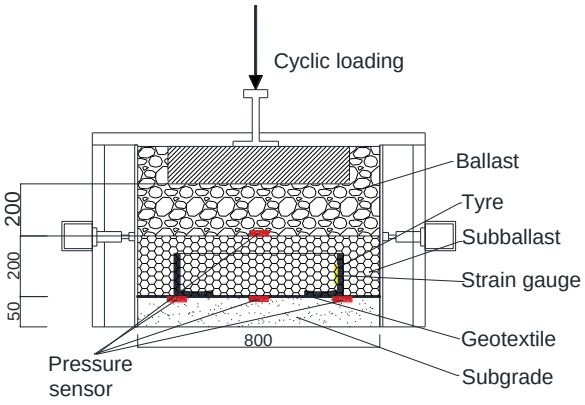


Figure 17 Schematic illustration of the prismoidal triaxial box (Indraratna et al. 2017c; with permission from ASCE)

### 3.2.2 Test Results

Figure 18 shows the cyclic loading test results in terms of the lateral displacement and vertical settlement of the specimens where lateral displacement without a tyre cell increases rapidly at the beginning of the test and then stabilises around N=100,000 cycles. As expected, there is a dramatic reduction in the lateral movement of the specimen confined with a tyre cell because this additional confinement causes the infilled capping layer particles to contract more under a higher confining pressure. The vertical settlement of these specimens varies with the number of loading cycles, as also shown in Figure 18. Here the vertical settlement develops rapidly during the first thousands of loading cycles and then gradually stabilises after 100,000 cycles. Note that the specimen reinforced with a tyre cell experiences a greater reduction in vertical displacement (around 10-12 mm) than the specimen without a tyre cell. Overall, these test results indicate confinement by a tyre cell will reduce track settlement and lateral displacement.

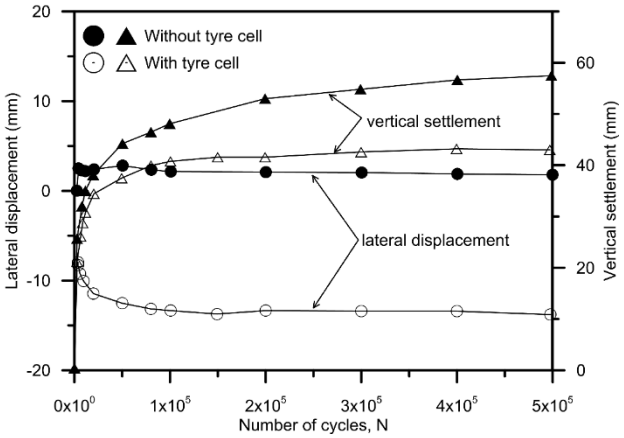


Figure 18 Lateral displacement and vertical settlement of the test specimens (modified from Indraratna et al. 2017c)

During loading and unloading, visco-elastic materials such as ballast exhibit hysteresis behaviour which can be evaluated by the damping ratio and dissipated energy. Figure 19 (a) shows a typical hysteresis loop obtained during the cyclic loading tests and the corresponding equations needed to calculate the damping ratio and dissipated strain energy. The damping ratio and dissipated energy of the capping layer confined with and without a tyre cell are shown in Figure 19 (b).

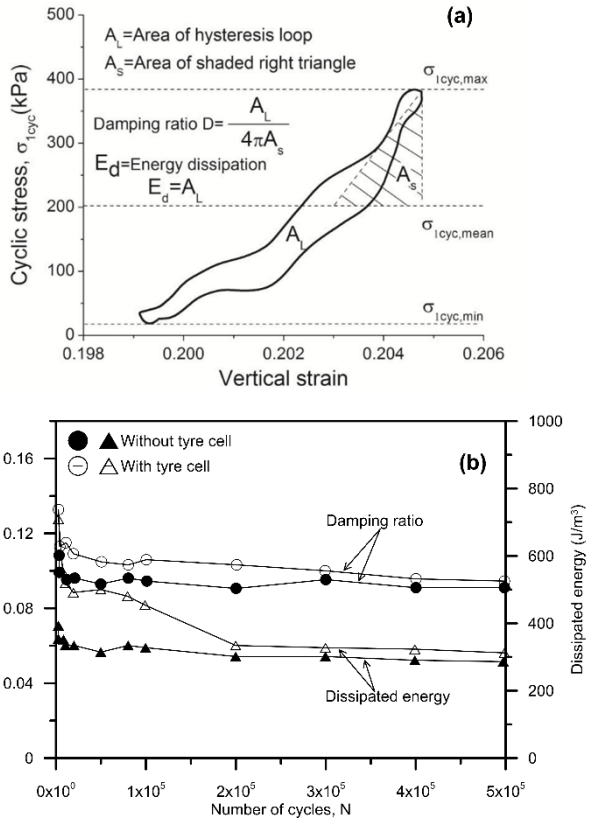


Figure 19 (a) Typical hysteresis loop showing the definition of damping ratio and energy dissipation (N=500,000); (b) variations in the damping ratio and dissipated energy with the number of cycles under different test conditions (modified after Indraratna et al. 2017c)

The test results show that when track is confined by a rubber tyre cell, the damping property is enhanced, and accordingly the dissipated energy increases. As the test begins, the damping ratio and the dissipated energy decrease as the number of loading cycles increase due to the high dissipation of energy by plastic sliding and particle breakage, but when the loading cycles are more than 10,000, the damping ratio and dissipated energy become almost constant as the granular mass becomes dense and stable. This is an important finding because any increase in energy dissipation can reduce the deterioration of track elements, and hence reduce the frequency and cost of track maintenance.

Ballast could undergo significant degradation during long-term service due to repeated impact loading (Indraratna et al. 2011), but intuitely, with a higher damping property, tyre cells will reduce ballast degradation. The Ballast Breakage Index (BBI) is used to evaluate the particle breakage of ballast. The particle size distribution curves (PSD) before and after the test, and the BBI values of specimens with and without a

tyre cell shown in Figure 20 indicate that the biggest change in the size of ballast takes place in the 37.5 mm sieve. The BBI of the specimen confined with a tyre cell is less than half of the specimen without tyre cell, which indicates that the inclusion of a tyre cell will definitely reduce the degradation of ballast. This result also suggests that the ballast layer could become more durable if rubber tyres are used, and thus reduce the amount of aggregates taken from the quarry.

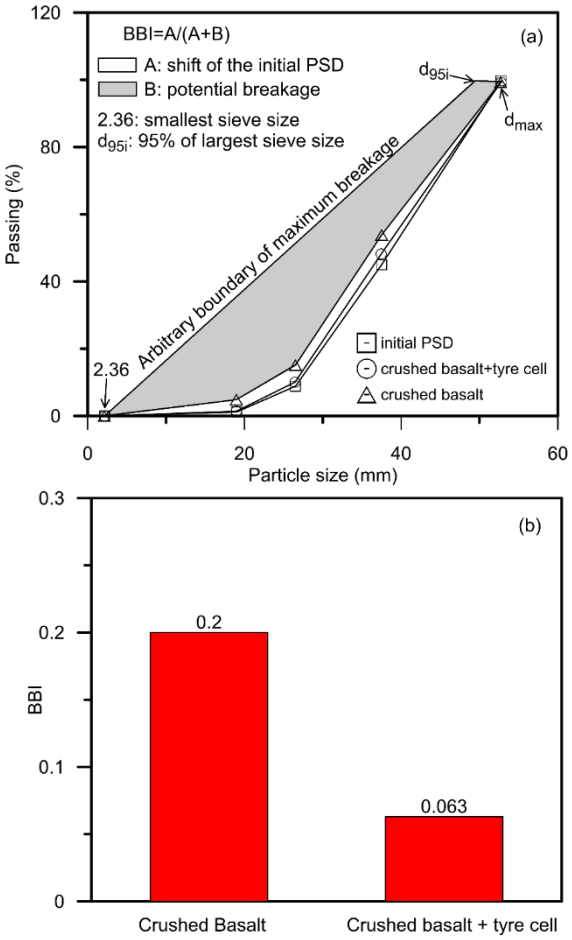


Figure 20 (a) Initial and final particle size distribution curves (PSD) of the specimens with and without tyre cell; (b) BBI of the specimens with and without tyre cell (modified from Indraratna et al. 2017c)

## 4. FINITE ELEMENT ANALYSIS

### 4.1 FEM for Under Sleeper Pats

#### 4.1.1 Model Geometry and Material Properties

In this finite element (FE) analysis, the unit cell of a rail track substructure (prototype sample) replicated in the prismoidal chamber during the laboratory experiment has been modelled; a full size model of the unit cell and its dimensions are shown in Figure 5. To optimise computational time, only one quarter of the unit cell is modelled in FEM analysis by exploiting the symmetry of the unit cell in each perpendicular direction in the horizontal plane (Figure 21). The boundary conditions are applied based on the actual laboratory triaxial chamber and by considering geometrical symmetry. In this numerical analysis, 25t and 35t axle loads with a loading frequency of 15 Hz are simulated with and without USP. FE analyses are only carried out up to 10,000 load cycles for each set of simulations by considering the time needed to solve a 3-D finite element problem under a large number of cyclic loadings.

The ballast and subballast are modelled as elasto-plastic material with non-associative behaviour while obeying the Drucker-Prager yield criterion (Drucker and Prager 1952). The material parameters for the Drucker-Prager model come from current and previous laboratory triaxial testing carried out on ballast and subballast materials obtained from the Bombo quarry, New South Wales (Indraratna et al. 2011). The concrete sleeper and under sleeper pad (USP) are modelled as linear elastic material. The material properties used for the FE simulation are summarised in Table 1.

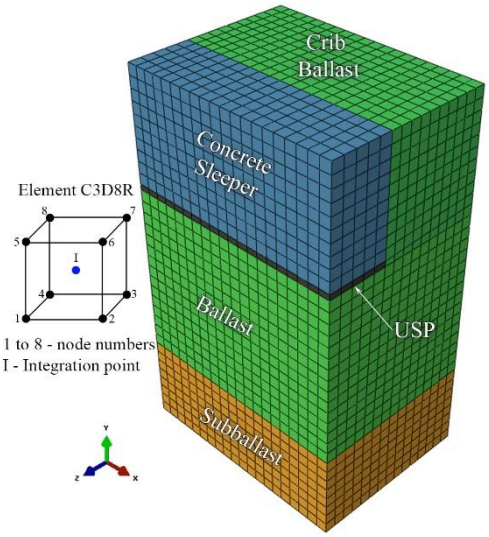


Figure 21 FE mesh for simulation and type of element (modified after Navaratnarajah et al. 2018)

Table 1 Material Properties for FE Analysis

| Material / Property | Ballast | Subballast | Concrete Sleeper | Under Sleeper Pad (USP) |
|---|---|---|---|---|
| Density, $\gamma$ (kg/m$^3$) | 1560 | 2115 | 2400 | 420 |
| Elastic Modulus, $E$ (MPa) | 125 | 100 | 36000 | 6 |
| Poisson's Ratio, $\nu$ | 0.25 | 0.3 | 0.2 | 0.48 |
| Friction Angle, $\phi$ (degrees) | 45 | 38 | - | - |
| Angle of Dilation, $\psi$ (degrees) | 15 | 9 | - | - |

### 4.1.2 FEM Mesh Generation and Element Type

The FE model is meshed using a structured pattern consisting of 3-D, 8-noded linear brick, and reduced integration (C3D8R) hexahedral elements. The mesh with different types of substructural layers is shown in Figure 21. The vertical size of the USP elements are seeded locally to match the thickness of the USP (i.e. 10 mm); all the other elements are >10mm or mostly equal to 20 mm thick cube elements.

### 4.1.3 FEM Results and Discussion

The vertical ($S_v$) and lateral ($S_h$) deformation of a 35 t axle load simulated at a cyclic loading frequency (f) of 15 Hz up to 10,000 load cycles are shown in Figures 22-23, respectively.

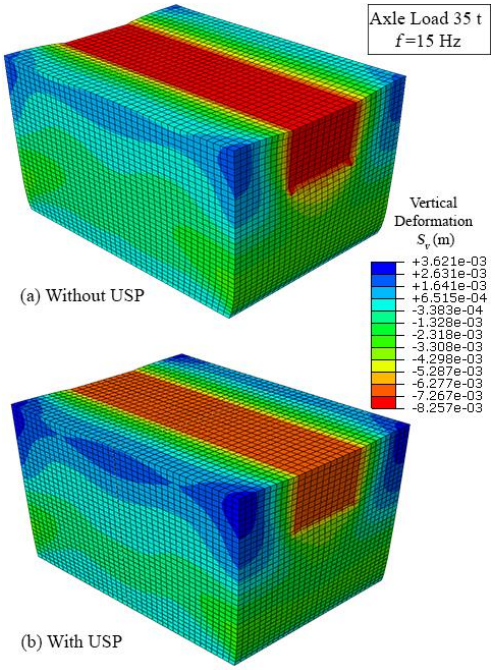


Figure 22 Vertical deformation contours predicted from FEM for 35t axle load at f=15 Hz; (a) without USP; (b) with USP (modified after Navaratnarajah et al. 2018)

Figures 22-23 show that maximum $S_v$ occurs in the vicinity of the loaded area of the sleeper. The ballast at the corners and longitudinal edges of the unit cell dilates because the crib ballast is not confined at the top and is free to move in a vertical direction (i.e. free boundary at the top). The magnitude of $S_v$ decreases along the depth of the substructure layers; while the magnitude of $S_h$ increases with depth, and the maximum $S_h$ occurs at a depth of 140-160 mm below the base of the sleeper and then decreases at a deeper part of the substructure. The maximum lateral displacement contours concentrate in the vicinity of one-half to two-thirds below the base of the sleeper. These results confirm that to reduce lateral spreading, the optimum location for any geo-inclusions (geogrids or geocells) within the ballast layer would be between one-half and two-thirds below the base of the sleeper. These results also confirm that USP placed under a concrete sleeper significantly reduces the vertical deformation of the substructure.

The average vertical ($S_v$) and lateral ($S_h$) deformation of the FE model and laboratory experiment are compared by plotting the variations of $S_v$ and $S_h$ against the number of cycles for 25t and 35t axle loads at f =15 Hz; the results are shown in Figures 24-25, respectively. The magnitude of $S_v$ increases as the axle load increases, whether there is or is not a USP. The predicted value of $S_v$ compares reasonably well with the experimental results, at least at the initial stages of the loading cycles ($N \leq 1000$). Cyclic strain hardening appears in the later stages of the loading cycles ($N > 1000$) as the deformation curve flattens with N, after about 1000 cycles. The degradation of ballast particles is not considered in this FE simulation, and this could be one reason for the difference in deformation between the experimental and numerical results where $N > 1000$, as well as the simplifications and approximations used in the numerical procedures. Nevertheless, the magnitude of $S_v$ is markedly reduced by the USP for 25t and 35t axle loads simulated at f=15 Hz, as captured well in this FEM simulation. The predicted $S_h$ by FE analysis confirms the laboratory findings that increasing the axle load from 25 to 35t increases the lateral spreading of ballast, whether with or without a USP.

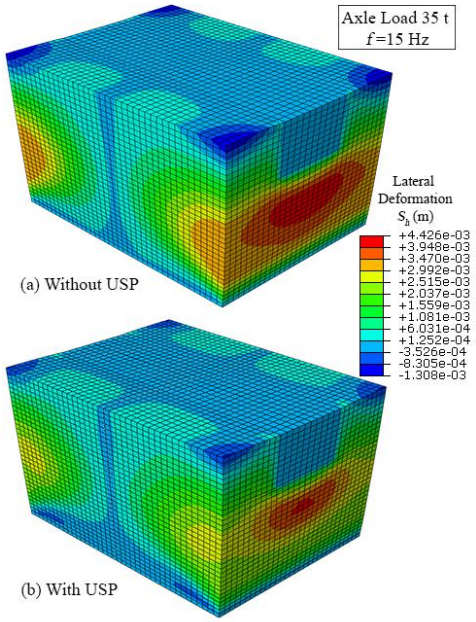


Figure 23 Lateral deformation contours predicted from FEM for 35t axle load at f=15 Hz; (a) without USP; (b) with USP (modified after Navaratnarajah et al. 2018)

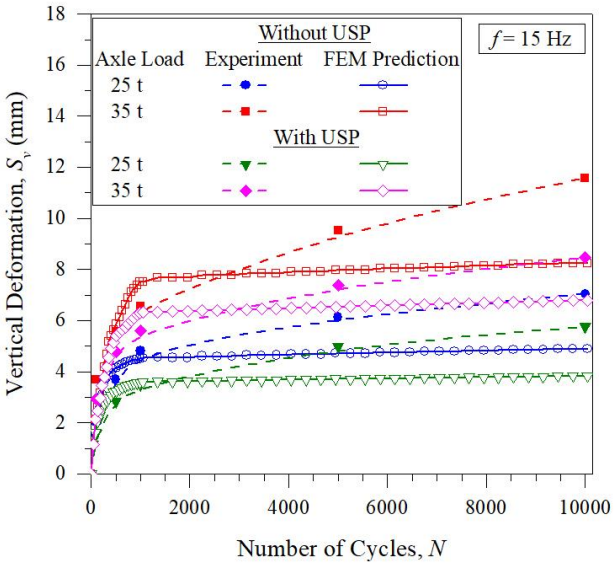


Figure 24 Variation of vertical deformation of ballast with N - Laboratory measurements vs. FE model prediction (modified after Navaratnarajah et al. 2018)

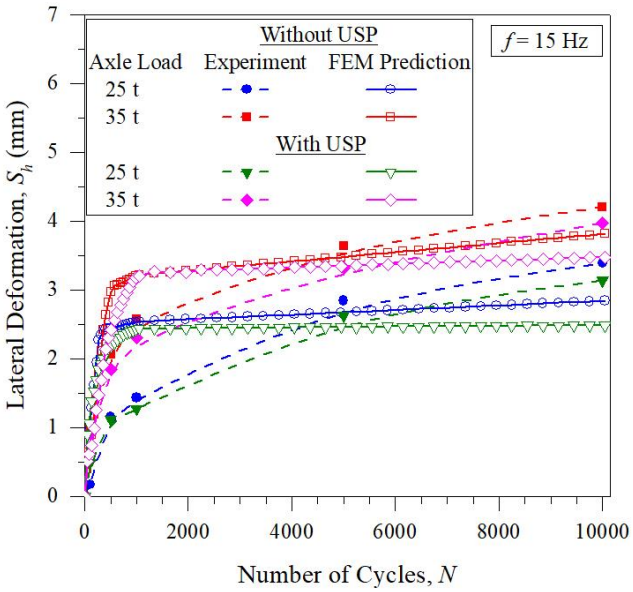


Figure 25 Variation of lateral deformation of ballast with N - Laboratory measurements vs. FE model prediction (modified after Navaratnarajah et al. 2018)

### 4.2 FEM for Tyre Cell-reinforced Subballast

FEM analysis is also used to examine the performance of a subballast capping layer reinforced with rubber tyres used to minimise track deformation and improve its bearing capacity. The commercially available FE software ABAQUS is used in this analysis. In this conventional railway track system, the steel rails are supported on reinforced concrete sleepers spaced at 0.60 m; the rail head is 0.075 m wide, the web is 0.018 m wide, and the base 0.15 m wide. The concrete sleepers are embedded into a layer of coarse granular aggregate (ballast). For a standard gauge track, a 2.50 m wide sleeper has been beveled to a maximum height of 0.20 m at the ends and 0.15 m at the centre. The ballast layer is 4 m wide at the base, 3 m wide at the crest, and 0.35 m high, and has a slope of 1:1. The subballast layer is confined by rubber tyres that are 6 m wide at the base and 0.25 m thick. A typical passenger car tyre is simulated as being 0.15 m wide, 0.56 m in diameter, and 0.01 m thick. The simulated geometry of the track is shown in Figure 26.

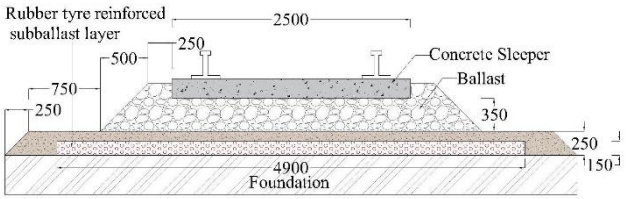


Figure 26 Track geometry with rubber tyres reinforced capping (subballast) layer (modified after Indraratna et al. 2017b)

This analysis is based on the heavy haul freight trains used by Australian railways to transport coal, construction materials, and aggregates. Traditionally, the axle load is 25t, which corresponds to a static wheel load of 122.5 kN. It is common practice to carry out a pseudo-static analysis in which the dynamic effects are considered by multiplying the static load by a dynamic amplification factor (DAF). In conventional practice, DAF is used as a function of the static (wheel) load and train velocity to obtain the equivalent dynamic load (Li and Selig 1998). The American Railway Engineering Association (AREA) recommends the expression for DAF = 1 + 0.0052 V/D, where V is the train velocity in kilometers per hour and D is wheel diameter in metres, A 25t axle load train moving at 100 km/h speed is simulated in this study.

#### 4.2.1 Materials Properties and Boundary Conditions

The ballast is modelled as linear elastic-perfectly plastic material with a Mohr-Coulomb failure criterion. The material parameters for the subballast, subgrade, and rubber tyre are shown in Table 2. The tyres are modelled as perfect cylinders, and contact between the tyres is considered smooth for simplicity. The sleepers and rails are modelled as non-yielding linear elastic material which is much stiffer than the ballast, the foundation, and the rubber tyres, to replicate a composite structure (Table 2). The FEM mesh with the subballast reinforced with rubber tyres consists of 22548 elements and 36761 nodes (Figure 27), while the model with unreinforced (no tyres) subballast only consists of 15050 elements and 24608 nodes. The ballasted track and foundation are meshed with hexahedral 8-noded elements with reduced integration points (C3D8R). Interaction between different layers of gravel is modelled with the same strategy used to simulate the unit cell. In order to simulate railway field conditions, a plane strain condition is applied to the model where the strain in a longitudinal direction is

considered insignificant compared to lateral transverse strain. By taking advantage of symmetry, only half of the embankment and foundation is modelled. The vertical planes along the outer edge of the foundation are constrained from lateral displacement in the x-direction, and the same constraint is affixed to the x-y planes to prevent lateral displacement in the z-direction. The base of the model is restricted from any displacement as conventionally required for an FEM mesh, i.e. a non-displacement bottom boundary as shown in Figure 27.

Table 2 Track variable values used in the numerical analysis

| | |
|---|---|
| **Rail Properties** | |
| Density (kg/m3) | 2,000 |
| Young's modulus E (MPa) Poisson's ratio, m | 500,000 |
| Poisson's ratio, m | 0 |
| **Sleeper Properties** | |
| Density (kg/m3) | 2,000 |
| Young's modulus E (MPa) | 30,000 |
| Poisson's ratio, m | 0 |
| **Ballast Layer** | |
| Density (kg/m3) | 1,530 |
| Young's modulus E (MPa) | 2 |
| Poisson's ratio, m | 0 |
| Internal angle of friction, / (degrees) | 45 |
| Angle of dilation, w (degrees) | 15 |
| Cohesion, c (kPa) | 1 |
| Thickness (m) | 0 |
| **Subballast Layer** | |
| Density (kg/m3) | 2,100 |
| Young's modulus E (MPa) | 2 |
| Poisson's ratio, m | 0 |
| Internal angle of friction, / (degrees) | 39 |
| Angle of dilation, w (degrees) | 15 |
| Cohesion, c (kPa) | 1 |
| **Subgrade Layer** | |
| Density (kg/m3) | 1,700 |
| Young's modulus E (MPa) | 2 |
| Poisson's ratio, m | 0 |
| Internal angle of friction, / (degrees) | 40 |
| Angle of dilation, w (degrees) | 15 |
| Cohesion, c (kPa) | 5 |
| **Tyre Properties** | |
| Density (kg/m3) | 1,500 |
| Poisson's ratio, m | 750 |
| Young's modulus E (MPa) | 0 |
| **Wheel Load** | |
| Static wheel load (kN) | 123 |
| Train Speed (km/h) | 100 |
| Dynamic amplification factor (DAF) | 2 |
| Dynamic wheel load (kN) | 188 |
| **Interface Elements** | |
| Normal property | Hard |
| Tangential coefficient | 0 |

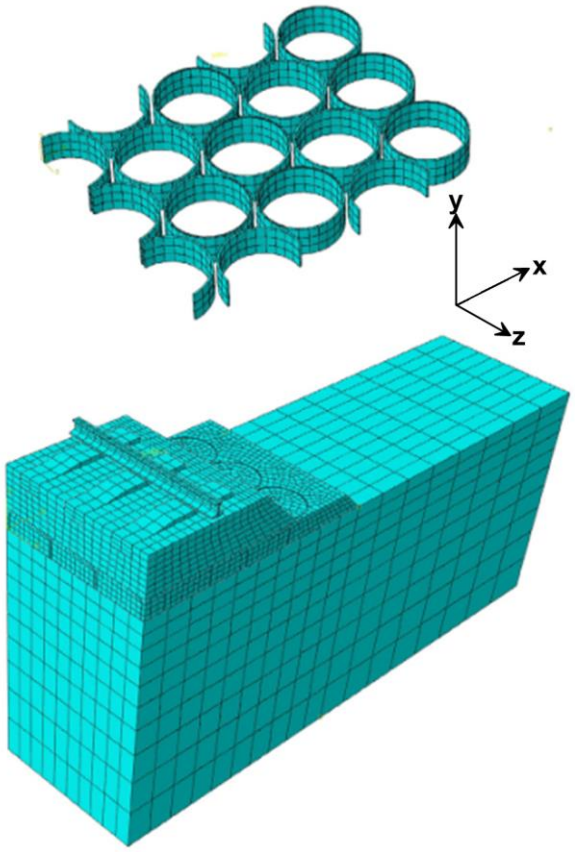


Figure 27 FEM mesh of ballasted railway track and foundation reinforced with rubber tyres in the subballast layer (modified after Indraratna et al. 2017b)

### 4.2.2 FEM Analysis Predictions

In Railway engineering, the design is mainly based on limiting the traffic and load-induced deviator stress in the subgrade to levels that will protect the subgrade from progressive shear failure and excessive plastic deformation (Li and Selig 1998). In order to maintain the track profile, ballast displacement (vertical and lateral) should be controlled within certain limits. This section of the paper will demonstrate how the subgrade deviator stress and ballast displacement can be influenced by using rubber tyres as reinforcement, unlike the unreinforced case. The input parameters used for the Finite Element Method analysis are listed in Table 2; note that three sleepers are considered to be sufficient for the analysis, and the deviator stress discussed is directly under the central sleeper.

The FEM analysis predictions are shown in Figures 28-30. Figure 28 shows the effect that reinforcement offered by rubber tyres has on the deviator stress at the surface of the subgrade. As expected, the highest deviator stress occurs near the sleeper end and then decreases towards the centre. This is consistent with the field observations where the largest subgrade depressions usually occur near the edges of the sleepers (Li and Selig 1998). With tyre reinforcement, a train running with the same axle load (i.e. 25t) and speed (i.e. 100 km/h), experiences a maximum deviator stress of 46.2 kPa,

which is almost a 12% reduction compared to an unreinforced section. Intuitively, the confining effect causes the tyres and gravel infill composite to act like a stiffer, flexible "mattress" which allows a reduced and more uniform stress to be transmitted to the subgrade. As shown in Figure 27, the area over which the traffic and load-induced subgrade stress is distributed is wider than the area without tyre reinforcement. Figure 29 shows the effect that tyre reinforcement has on the distribution of deviator stress with the depth of subgrade. Here, the deviator stress decreases with the depth of the subgrade. There is a huge reduction in the deviator stress within a depth of 0-0.7 m by reinforcing the subballast layer with a tyre cell, and when the depth is more than 0.7 m, the deviator stress of the subgrade is similar for unreinforced and reinforced track.

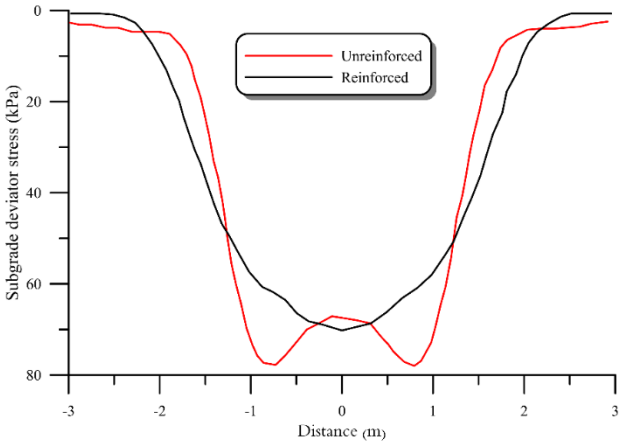


Figure 28 Subgrade stress distribution below the reinforced and unreinforced track (modified after Indraratna et al. 2017b)

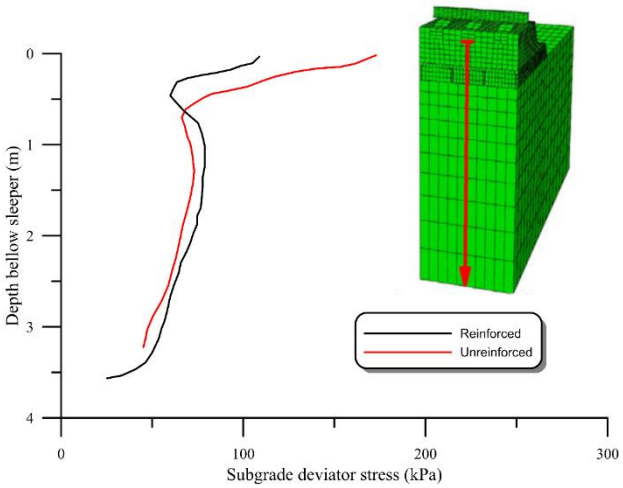


Figure 29 Distribution of subgrade deviator stress with depth for reinforced and unreinforced track (modified after Indraratna et al. 2017b)

The numerical predictions of lateral displacement along the slope of the embankment are shown in Figure 30, where the lateral deformation is reduced considerably due to reinforcement by the tyre cell. The largest lateral movement of subballast develops beneath the edge of the sleeper for reinforced subballast.

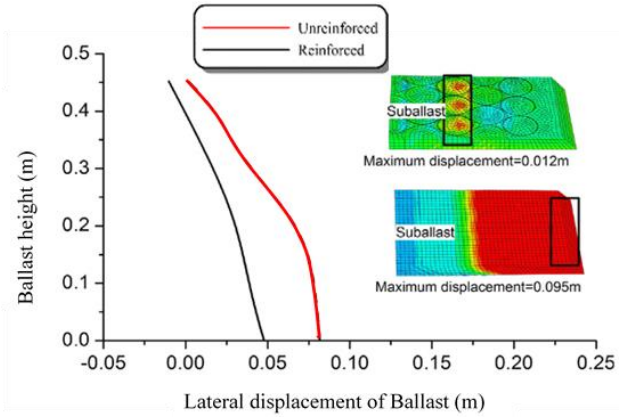


Figure 30 FEM predictions of lateral displacement for reinforced and unreinforced rail track (modified after Indraratna et al. 2017b)

## 5. CONCLUSIONS

This paper presented some innovative ways of using energy absorbing waste tyre products in rail tracks such as rubber crumbs blended with mining waste (i.e. SFS and CW) to replace traditional subballast, using under sleeper pats (USP) or under ballast mats (UBM) to minimise ballast deformation and degradation, and using waste tyre cells to reinforce the subballast layer. A schematic selection was used to optimise the SFS+CW+RC mixtures for subballast. Large scale cubical triaxial tests were carried out to examine the performance of USP, UBM and tyre cells in a track system. FEM analysis was also used to simulate the application of USP and tyre cells in railway under field conditions. Significant findings can be drawn from this paper:

- The SFS+CW+RC matrix with SFS:CW=7:3 and 10% RC (mixed by weight) was selected to be the optimal mixture for subballast because it has much higher energy absorbing capacity, sufficient shear strength, and acceptable deformation. The energy absorbing analysis showed that the proposed optimal waste matrix can be a promising synthetic energy absorbing layer to help minimise track degradation.
- The large scale triaxial tests showed promising outcomes in the reduction of stress, vertical and lateral strain, and the degradation of ballast stabilised with USP in open track or stiff subgrade conditions. For instance, by using USPs under open track conditions, vertical deformation decreased from 19%–29% for the 25-t axle load, and about 21% for the 35t axle load, and the lateral deformation of the ballast decreased between 9%–14% and 9%–11% for 25 and 35t axle loads, respectively. Ballast degradation decreased significantly after installing USPs at the sleeper-to-ballast interface. The top ballast layer experienced higher particle breakage than the middle and bottom layers. On average, when all three layers are considered, USPs reduced the BBI by

more than 50%. Although particle breakage of ballast was not incorporated in the 3D FE analysis, the vertical and lateral deformation predicted in the ballast layer generally agreed with the experimental findings.

- The tests of ballasted track stabilised with UBM on a very stiff subgrade confirmed the ballast experienced considerably less deformation and degradation. The vertical and lateral plastic deformation, and the breakage of ballast, increased with the axle loads and train speed. An approximate 10–20% reduction in vertical plastic deformation, an approximate 5–10% reduction in lateral plastic deformation, and a substantial 35-45% reduction in ballast breakage were observed as favourable outcomes.
- Large-scale laboratory testing and FEM modelling of a capping layer reinforced with rubber tires showed they helped to reduce the stress transmitted to the subgrade and increased the energy dissipation capacity; in fact the recycled tires increased the stiffness of the capping layer by approximately 50%, reduced the breakage of ballast aggregates by more than half, and also minimised the lateral deformation and vertical settlement by more than 10 mm compared to the unreinforced track.

**Acknowledgements:**

The Authors wish to acknowledge the Australian Research Council (ARC) and Industry partners for providing support through the ARC Industrial Transformation Training Centre for Advanced Technologies in Rail Track Infrastructure (ITTC-Rail) as well as the support for the ARC Discovery project (DP180101916). The efforts of current and past postdoctoral research fellows and academic staff Dr. Qideng Sun, A/Prof. Jayan Vinod, and A/Prof. Cholachat Rujikiatkamjorn that have contributed to the contents of this Keynote paper are also gratefully appreciated. The Authors sincerely acknowledge Rail Manufacturing Cooperative Research Centre (funded jointly by participating rail organisations and the Australian Federal Government's Business Cooperative Research Centres Program) through two Projects, R2.5.1 and R2.5.2. The authors also thank the Australasian Centre for Rail Innovation (ACRI), Tyre Stewardship Australia (TSA), Global Synthetics Pty Ltd, Naue GmbH & Co. KG, Foundation Specialists Group, Sydney Trains (formerly RailCorp), Australian Rail Track Corporation (ARTC), Bridgestone Corporation, Ecoflex International Pty Ltd, South 32, ASMS, among others. The cooperation of David Christie (formerly Senior Geotechnical Consultant, RailCorp), Tim Neville (ARTC), Michael Martin (Aurizon/QLD Rail) and Jim Grant (Ecoflex) during these industry linkages is gratefully appreciated. Salient contents from these previous studies are reproduced herein with kind permission from the original sources, including ASCE-Journal of Geotechnical and Geoenvironmental Engineering, Transportation Geotechnics, ASCE- Journal of Materials in Civil Engineering among others. The authors are also grateful to UOW technical staff, namely, Alan Grant, Cameron Neilson, Duncan Best, Richard Berndt and Ritchie McLean for their assistance during laboratory testing.

## References:

AS-2758.7 (2015). Aggregates and rock for engineering purposes, Part 7: Railway ballast. Sydney, New South Wales, Australia, Standard Australia.

ASTM-D6270 (2008). Standard practice for use of scrap tires in civil engineering applications-ASTM D 6270-98 (re-approved in 2008), ASTM W. Conshohocken, PA.

Costa, P. A., Calçada, R. and Cardoso, A. S. (2012). "Ballast mats for the reduction of railway traffic vibrations. Numerical study." *Soil Dynamics and Earthquake Engineering*, **42**, 137-150.

Drucker, D. C. and Prager, W. (1952). "Soil mechanics and plastic analysis or limit design." *Quarterly of applied mathematics*, **10**(2), 157-165.

Edil, T. B. and Bosscher, P. J. (1994). "Engineering properties of tire chips and soil mixtures." *Geotechnical testing journal*, **17**(4), 453-464.

Feng, Z.-Y. and Sutter, K. G. (2000). "Dynamic properties of granulated rubber/sand mixtures." *Geotechnical Testing Journal*, **23**(3), 338-344.

Ferreira, T. M., Teixeira, P. F. and Cardoso, R. (2010). "Impact of bituminous subballast on railroad track deformation considering atmospheric actions." *Journal of Geotechnical and Geoenvironmental Engineering*, **137**(3), 288-292.

Hunt, G. and Wood, J. (2005). "Review of the effect of track stiffness on track performance." *RSSB, Research Project*, **372**.

Indraratna, B., Biabani, M. M. and Nimbalkar, S. (2014). "Behavior of geocell-reinforced subballast subjected to cyclic loading in plane-strain condition." *Journal of Geotechnical and Geoenvironmental Engineering*, **141**(1), 04014081.

Indraratna, B., Ferreira, F. B., Qi, Y. and Ngo, T. N. (2018). "Application of geoinclusions for sustainable rail infrastructure under increased axle loads and higher speeds." *Innovative Infrastructure Solutions*, **3**(1), 69.

Indraratna, B., Lackenby, J. and Christie, D. (2005). "Effect of confining pressure on the degradation of ballast under cyclic loading."

Indraratna, B., Ngo, N. T. and Rujikiatkamjorn, C. (2012). "Deformation of coal fouled ballast stabilized with geogrid under cyclic load." *Journal of Geotechnical and Geoenvironmental Engineering*, **139**(8), 1275-1289.

Indraratna, B., Qi, Y. and Heitor, A. (2017a). "Evaluating the properties of mixtures of steel furnace slag, coal wash, and rubber crumbs used as subballast." *Journal of Materials in Civil Engineering*, **30**(1), 04017251.

Indraratna, B., Qi, Y., Ngo, T. N., Rujikiatkamjorn, C., Neville, T., Ferreira, F. B. and Shahkolahi, A. (2019). "Use of Geogrids and Recycled Rubber in Railroad Infrastructure for Enhanced Performance." *Geosciences*, **9**(1), 30.

Indraratna, B., Salim, W. and Rujikiatkamjorn, C. (2011). Advanced rail geotechnology–ballasted track, CRC press.

Indraratna, B., Sun, Q. and Grant, J. (2017b). "Behaviour of subballast reinforced with used tyre and potential application in rail tracks." *Transportation Geotechnics*, **12**, 26-36.

Indraratna, B., Sun, Q., Heitor, A. and Grant, J. (2017c). "Performance of rubber tire-confined capping layer under cyclic loading for railroad conditions." *Journal of Materials in Civil Engineering*, **30**(3), 06017021.

Jayasuriya, C., Indraratna, B. and Ngo, T. N. (2019). "Experimental Study to Examine the Role of Under Sleeper Pads for Improved Performance of Ballast under Cyclic Loading." *Transportation Geotechnics*.

Jeffs, T. and Tew, G. (1991). A Review of Track Design Procedures-Sleepers and Ballast, Vol. 2, Railways of Australia, Australian Government Publishing Service, Melbourne.

Kim, H.-K. and Santamarina, J. (2008). "Sand–rubber mixtures (large rubber chips)." *Canadian Geotechnical Journal*, **45**(10), 1457-1466.

Lackenby, J., Indraratna, B., McDowell, G. and Christie, D. (2007). "Effect of confining pressure on ballast degradation and deformation under cyclic triaxial loading."

Li, B., Huang, M. and Zeng, X. (2016). "Dynamic behavior and liquefaction analysis of recycled-rubber sand mixtures." *Journal of Materials in Civil Engineering*, **28**(11), 04016122.

Li, D. and Selig, E. T. (1998). "Method for railroad track foundation design. I: Development." *Journal of Geotechnical and Geoenvironmental Engineering*, **124**(4), 316-322.

Navaratnarajah, S. K. and Indraratna, B. (2017). "Use of rubber mats to improve the deformation and degradation behavior of rail ballast under cyclic loading." *Journal of geotechnical and geoenvironmental engineering*, **143**(6), 04017015.

Navaratnarajah, S. K., Indraratna, B. and Ngo, N. T. (2018). "Influence of under sleeper pads on ballast behavior under cyclic loading: experimental and numerical studies." *Journal Geotechnical and Geoenvironmental Engineering*, **144**(9), 04018068.

Nimbalkar, S., Indraratna, B., Dash, S. K. and Christie, D. (2012). "Improved performance of railway ballast under impact loads using shock mats." *Journal of geotechnical and geoenvironmental engineering*, **138**(3), 281-294.

Qi, Y., Indraratna B., Heitor, A., Vinod, J.S. (2019b) The Influence of Rubber Crumbs on the Energy Absorbing Property of Waste Mixtures. In: Sundaram R., Shahu J., Havanagi V. (eds) Geotechnics for Transportation Infrastructure. Lecture Notes in Civil Engineering, vol 29, pp. 271-281. Springer, Singapore. DOI: 10.1007/978-981-13-6713-7_22.

Qi, Y., Indraratna, B., Heitor, A. and Vinod, J. S. (2017). "Effect of rubber crumbs on the cyclic behavior of steel furnace slag and coal wash mixtures." *Journal of Geotechnical and Geoenvironmental Engineering*, **144**(2), 04017107.

Schneider, P., Bolmsvik, R. and Nielsen, J. C. (2011). "In situ performance of a ballasted railway track with under sleeper pads." *Proceedings of the Institution of Mechanical Engineers, Part F: Journal of Rail and Rapid Transit*, **225**(3), 299-309.

Senetakis, K., Anastasiadis, A. and Pitilakis, K. (2012). "Dynamic properties of dry sand/rubber (SRM) and gravel/rubber (GRM) mixtures in a wide range of shearing strain amplitudes." *Soil Dynamics and Earthquake Engineering*, **33**(1), 38-53.

Sol-Sánchez, M., Moreno-Navarro, F. and Rubio-Gámez, M. C. (2015). "The use of elastic elements in railway tracks: A state of the art review." *Construction and building materials*, **75**, 293-305.

Suiker, A. S., Selig, E. T. and Frenkel, R. (2005). "Static and cyclic triaxial testing of ballast and subballast." *Journal of geotechnical and geoenvironmental engineering*, **131**(6), 771-782.

Sun, Q. D., Indraratna, B. and Nimbalkar, S. (2015). "Deformation and degradation mechanisms of railway ballast under high frequency cyclic loading." *Journal of Geotechnical and Geoenvironmental Engineering*, **142**(1), 04015056.